# Polar jets of swimming bacteria condensed by a patterned liquid crystal

Taras Turiv<sup>1</sup>, Runa Koizumi<sup>1</sup>, Kristian Thijssen<sup>2</sup>, Mikhail M. Genkin<sup>3</sup>, Hao Yu<sup>1</sup>, Chenhui Peng<sup>1</sup>, Qi-Huo Wei<sup>1,4</sup>, Julia M. Yeomans<sup>2</sup>, Igor S. Aranson<sup>5</sup>, Amin Doostmohammadi<sup>2</sup>, Oleg D. Lavrentovich<sup>1,4</sup>\*

## **Affiliation:**

<sup>1</sup>Advanced Materials Liquid Crystal Institute and Chemical Physics Interdisciplinary Program, Kent State University, Kent, OH 44242, USA

<sup>2</sup>The Rudolf Peierls Centre for Theoretical Physics, University of Oxford, Clarendon Laboratory, Parks Rd., Oxford, OX1 3PU, UK

<sup>3</sup>Cold Spring Harbor Laboratory, 1 Bungtown Rd, Cold Spring Harbor, NY 11724, USA

<sup>4</sup>Department of Physics, Kent State University, Kent, OH 44242, USA

<sup>5</sup>Department of Biomedical Engineering, Pennsylvania State University, University Park, Pennsylvania 16802, USA

## **Corresponding author:**

\*Author for correspondence: e-mail: olavrent@kent.edu, tel.: +1-330-672-4844.

Keywords: active matter, liquid crystals, living bacteria

#### Abstract

Active matter exhibits remarkable collective behavior in which flows, continuously generated by active particles, are intertwined with the orientational order of these particles. The relationship remains poorly understood as the activity and order are difficult to control independently. Here we demonstrate important facets of this interplay by exploring the dynamics of swimming bacteria in a liquid crystalline environment with predesigned periodic splay and bend in molecular orientation. The bacteria are expelled from the bend regions and condense into polar jets that propagate and transport cargo unidirectionally along the splay regions. The bacterial jets remain stable even when the local concentration exceeds the threshold of bending instability in a non-patterned system. Collective polar propulsion and the different roles of bend and splay are explained by an advection-diffusion model and by numerical simulations that treat the system as a two-phase active nematic. The ability of prepatterned liquid crystalline medium to streamline the chaotic movements of swimming bacteria into polar jets that can carry cargo along a predesigned trajectory opens the door for potential applications in microscale delivery and soft microrobotics.

Active matter, an out-of-equilibrium assembly of moving and interacting objects that locally convert energy into directed motion, shows an intriguing interplay of dynamics and spatial order  $^1$ . In the so-called active nematics, this order is orientational, naturally associated with the vector character of velocity and with the elongated shape of moving units  $^2$ . A conventional (passive) nematic exhibits a long-range orientational order along an axis of anisotropy called the director  $\hat{\bf n} \equiv -\hat{\bf n}$ . The passive nematic can be transformed into a "living nematic", a subclass of active nematics, by dispersing active particles in it, such as swimming bacteria  $^3$ . The director, either uniform  $^{3-6}$ , or spatially distorted  $^{3,6-9}$ , serves as an easy swimming pathway for bacteria. A living nematic allows one to control independently the activity, through concentration and speed of bacteria  $^{3,10}$  and orientational order, through predesigned director patterns  $^{6,7}$ . This tunability is important for better understanding of active systems, as the coupling of the orientational order and activity is at the core of current theoretical modeling  $^{1,2,10-19}$ .

In theoretical modeling, the active matter is usually considered as incompressible, with the active units as the only ingredient, filling the space fully. As a result, the predicted activitytriggered macroscopic flows involve the entire sample with all its material points. However, in real experimental systems, there is often some space left for the passive background. One intriguing example <sup>20</sup> is active microtubules dispersed in a passive aqueous buffer in a volume proportion 1:1000. As shown by Wu et al <sup>20</sup>, when such a dilute, globally isotropic active fluid is confined into a macroscopic 3D channel, it flows in absence of any external pressure gradients, thanks to the formation of a thin active nematic wetting layer at the bounding surface; the bulk remains isotropic. The concentration of active microtubules in this system is thus not necessarily uniform in space. The living nematic is another example where a spatially non-uniform distribution of concentration and thus activity can be induced. For example, in <sup>7,8</sup> the swimming bacteria were demonstrated to gather near defects of a positive topological charge in a passive nematic background and to avoid defects with negative charges <sup>7-9</sup>. The dispersed nature and the possibility of deterministic spatially varying concentration of active units in these two systems add richness to the idealized model of an incompressive active matter. Moreover, in living nematics with a prepatterned  $\hat{\mathbf{n}}$ , there is an interesting interplay of activity and geometry: patterns with a pure splay or pure bend of  $\hat{\bf n}$  support bipolar swimming of bacteria parallel to  $\hat{\bf n}$ , while configurations with an inseparable equal mix of splay and bend cause unipolar circulation of bacterial swarms at some angle to the pre-inscribed  $\hat{\bf n}^7$ .

Splay and bend are known to affect differently some aspects of active nematics. For example, a system of "pushers", such as the swimming bacteria, at weak levels of activity develops spontaneous bend <sup>3,11,21</sup>, while "pullers" are expected to develop splay <sup>21</sup>. Simulations <sup>13,15,16</sup> predict that a medium-level activity triggers more complex distortions, such as "kink walls" <sup>15</sup> in which the director field resembles rows and columns of letters "C". In these kink walls, splay (at the ends of C's) and bend (in the middle of C's) coexist and alternate with each other in a plane of the sample. It was also demonstrated <sup>22,23</sup> that the effective splay and bend elastic moduli are renormalized by activity. However, it remains unknown whether and how the concentration of active units in dispersed systems is coupled to splay and bend.

In this work, in order to understand the interplay of the concentration field of active units and splay-bend deformations of the orientational order, we explore a living nematic in which the passive director is predesigned into a periodic pattern of alternating splay and bend. We explore two different cases, a weakly concentrated system, in which the individual bacteria follow the patterned director, and a concentrated system, in which collective effects trigger bending instabilities of flows. The design allows us to uncover different effects of splay and bend on the concentration and swimming polarity of bacteria and to demonstrate a pathway to stabilize active flows against instabilities. In both systems, the director pattern forces a strongly non-uniform distribution of bacteria, condensing them into polar "jets" that move unidirectionally along the maximum splay. The bend regions are mostly deprived of the swimmers and serve (i) to reverse the polarity of bacterial trajectories, (ii) to expel the bacteria towards splay regions and (iii) to stabilize the shape of the condensed jets: the jets remain stable even when the concentration of bacteria in them exceeds (by an order of magnitude) the threshold of bend instability observed in a uniformly aligned cell. The concentration gradients and jets in the dilute limit are described by an advection-diffusion model that operates with two subsets of bacteria swimming in opposite directions 8. With an increase in bacterial concentration, the model of Refs. 8,9 exhibits the onset of undulations and instability of the jets. We further complement the experiments on the strongly concentrated system with numerical simulations of a two-phase model of active nematics to show that the difference between the bacterial response to splay and bend can be attributed to a generic mechanism of active concentration exchange between the two regions and to demonstrate the enhanced stability of the condensed jets against bending. We hope that the results will stimulate further theoretical models that allow the concentration and activity to vary in space and time.

#### Results and discussion

The living nematic represent a water-based chromonic nematic disodium cromoglycate (DSCG) with dispersed bacteria *Bacillus subtilis*. We explore diluted (spatially averaged concentration  $\langle c \rangle \approx 0.3 \times 10^{14} \text{ m}^{-3}$ ) and concentrated ( $\langle c \rangle \approx 1.5 \times 10^{14} \text{ m}^{-3}$ ) dispersions. The living nematic is confined by two glass plates separated by a gap  $h = 20 \,\mu\text{m}$  (Fig. 1a). The surfaces of the two plates are photoaligned to produce identical director patterns <sup>7,24</sup>. To facilitate the presentation, we consider the director of the passive nematic as a vector, which is permissible in the absence of disclinations <sup>25</sup>. The photopatterned vector field written in Cartesian coordinates as

$$\hat{\mathbf{n}}_0 = [n_x, n_y, n_z] = \left[\cos(\pi y / L), -\sin(\pi y / L), 0\right],\tag{1}$$

represents a one-dimensionally modulated splay and bend in the xy-plane of the cell (Fig. 1b,c);  $L = 160 \,\mu\text{m}$ . The pattern resembles rows of letters "C" and thus can be called "C-stripes". Pure splay deformations are located at  $y = 0, \pm L, \pm 2L,...$ , while bend at  $y = \pm L/2, \pm 3L/2,...$ 

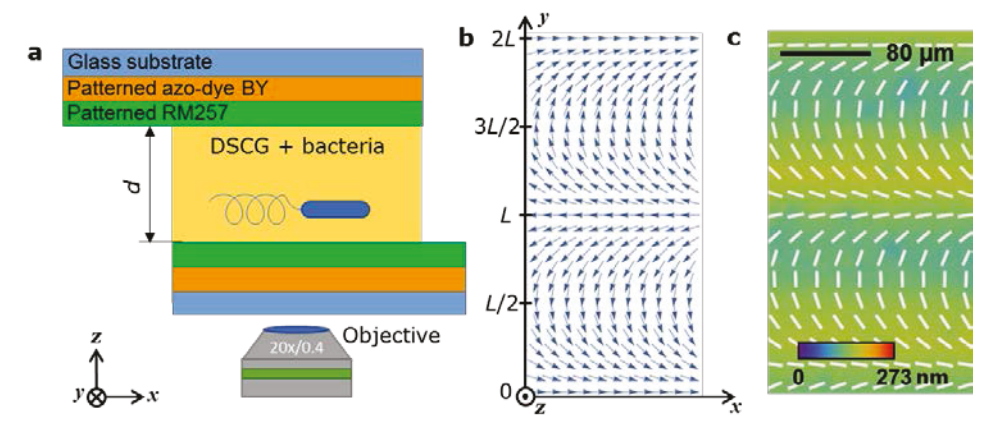


**Fig. 1**. Experimental scheme of the cell with bacteria swimming in a patterned nematic DSCG. **a**, Schematics of the experimental setup and liquid crystal cell. **b**, Predesigned director field  $\hat{\mathbf{n}}_0$ . **c**, Optical phase retardation (background colors) and director field of the photopatterned nematic DSCG at 24°C mapped by the PolScope (see Methods).

# Weakly concentrated dispersion

Once the dispersion is injected into the patterned cell, the swimming bacteria start to leave the bend regions and accumulate in the splay regions, moving predominantly along the positive direction of the x-axis (Fig. 2a,b), i.e., along the vector  $\mathbf{s} = -\hat{\mathbf{n}}_0 \nabla \cdot \hat{\mathbf{n}}_0$ . The bacterial concentration c, calculated by averaging over the x-axis, is strongly modulated along the y-axis; see time evolution of c(y) in Fig. 2c. The distribution  $\langle c(y) \rangle_t$  averaged over 10 min, is of the same period

L as the splay-bend pattern; in the splay regions,  $c(y) \approx 4.4 \times 10^{-14} \text{ m}^{-3}$  (Fig. 2d), 15 times higher than the initial concentration  $\langle c \rangle \approx 0.3 \times 10^{14} \text{ m}^{-3}$ .

The velocity field of bacteria is biased towards the converging splay  $\mathbf{s}$  (Fig. 2e,f and Supplementary Video 1). If an individual bacterium happens to swim in the opposite direction, the diverging  $\hat{\mathbf{n}}_0$  forces it to make a U-turn by swimming through the bend along  $\hat{\mathbf{n}}_0$  and then joining a bacterial jet moving along the x-axis in the neighboring splay region. The velocity components  $v_x(y)$  and  $v_y(y)$  are strongly modulated along the y-axis (Fig. 2g);  $v_x(y)$  is predominantly positive, reflecting polar transport along the x-axis, while  $v_y(y)$  fluctuates near zero, demonstrating absence of net flows along the y-axis.

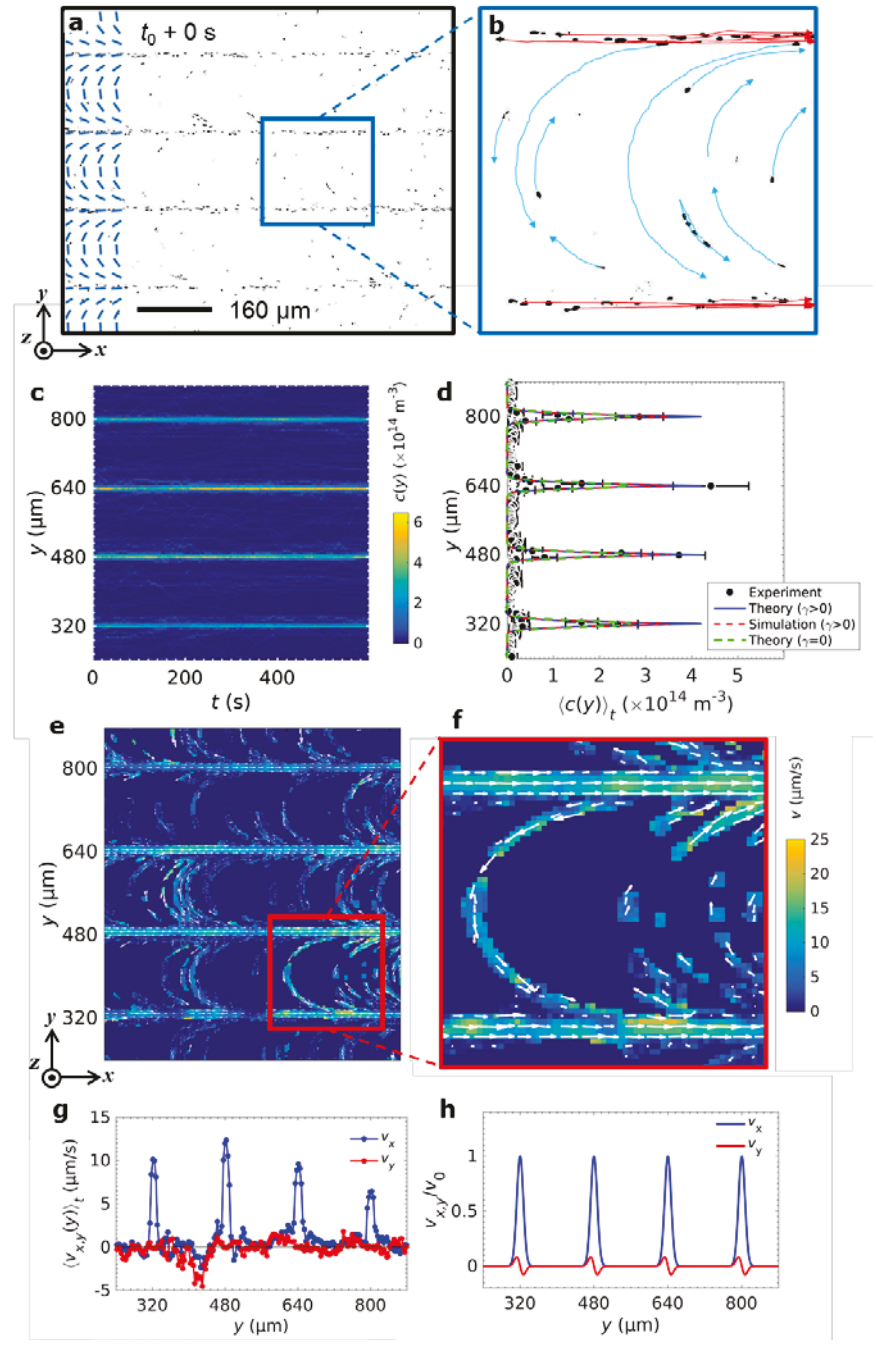


**Fig. 2.** Trajectories, distribution and velocities of the bacteria in a dilute living nematic,  $\langle c \rangle \approx 0.3 \times 10^{14} \, \mathrm{m}^{-3}$ , controlled by a periodic splay-bend director pattern. **a,b**, Enhanced (by subtracting the average image over all frames of the video) microscopic images of bacteria condensed in the splay regions; part **b** shows trajectories of bacteria moving in splay (red lines) and crossing the bend (blue curves with the arrows indicating the direction of swimming). **c**, Kymograph of the concentration c(y) with the time step 0.5 s. **d**, Time average of bacterial concentration  $\langle c(y) \rangle_t$  (errors are standard deviations (SD) of concentration) fitted with the theoretical curves c(y) obtained using equation (4) for the finite director anchoring,

 $\gamma / a = 5 \times 10^{-2} \, \mathrm{m}^3/\mathrm{N}$ , and calculated from equation (6) for no director realignment regime,  $\gamma = 0$ ; other parameters are set as  $v_0 = 10 \, \mathrm{\mu m/s}$ ,  $D_c = 10 \, \mathrm{\mu m}^2/\mathrm{s}$ ,  $L = 160 \, \mathrm{\mu m}$ ,  $U_0 = 10^{-17} \, \mathrm{N} \, \mathrm{m}$ , and  $C_0 = 1.23 \times 10^{-8} \, \mathrm{m}^{-3}$ ; all curves are calculated for an infinite reversal time  $\tau$  (see SI for details). **e,f**, Experimental velocity map; the length of arrows and the pseudocolors scale linearly with the speed of bacteria. **g**, Experimental velocity components  $v_x(y)$  and  $v_y(y)$ . **h**, Velocity components, weighted by the concentrations of bacteria swimming parallel  $c^+$  and antiparallel  $c^-$  to the vector  $\hat{\mathbf{n}}_0$ ,  $v_{x,y} = v_{x,y}^+ c^+ + v_{x,y}^- c^-$ , obtained from the advection-diffusion simulation, normalized by the maximum velocity  $v_0$ . All data are averaged over 600 s. See Supplementary Video 1.

Condensation of bacteria in the splay regions and formation of polar jets follow from the preference of bacteria to swim along  $\hat{\mathbf{n}}_0$ . Swimming along any other direction involves penalties associated with increased viscous resistance, bulk elastic and surface anchoring energy cost <sup>26</sup>. To describe the effect, we employ the model of Genkin et al <sup>8</sup>, in which transport of bacteria in a nematic is governed by two depth-averaged coupled advection-diffusion equations for the concentrations  $c^{\pm}$  of bacteria swimming parallel ( $c^{+}$ ) or anti-parallel ( $c^{-}$ ) to  $\hat{\mathbf{n}} = (n_x, n_y, 0)$ :

$$\partial_t c^{\pm} + \nabla \cdot \left( \pm v_0 \hat{\mathbf{n}} c^{\pm} + \mathbf{v}_f c^{\pm} \right) = \mp \frac{c^+ - c^-}{\tau} + D_c \nabla^2 c^{\pm}; \tag{2}$$

here  $v_0 \sim 10 \, \mu\text{m/s}$  is the bacterium swimming speed,  $D_c \sim 10 \, \mu\text{m}^2/\text{s}$  is the concentration diffusion coefficient,  $\mathbf{v}_f$  is flow velocity and  $\tau$  is the swimming direction reversal time;  $\hat{\mathbf{n}}$  can differ from the prescribed  $\hat{\mathbf{n}}_0$  in Eq. (1) because of the torques and forces imposed by the bacteria. A direction reversal means that the bacterium leaves the population  $c^+$  and joins  $c^-$ , or vice versa.

Our experiments show that  $\tau \sim 10^4$  s (Supplementary Information (SI) and Supplementary Video 1) is much larger than the typical duration of the experiment. In the tumbling-free  $\tau \to \infty$  limit and for  $\mathbf{v}_f = 0$  (fluid velocity is small compared to the propulsion velocity), the equations for  $c^{\pm}$  decouple; integrating these stationary equations (2), one obtains

$$\pm v_0 n_y c^{\pm} = D_c \partial_y c^{\pm} + C_{1,2}. \tag{3}$$

We set constants  $C_{1,2}$  to zero to enforce the periodicity condition.

Bacterial activity imposes an active stress on the nematic  $\sigma_{\rm act} = -U_0 \mathbf{Q} (c^+ + c^-)$ , where "-" corresponds to pusher-like particles,  $U_0$  is the hydrodynamic force dipole strength of a bacterium<sup>8</sup>,

 $\mathbf{Q} = \hat{\mathbf{n}}\hat{\mathbf{n}} - \mathbf{I}/2$  is the tensor order parameter of the nematic, **I** is the identity tensor. The active stress generates a realigning force  $\mathbf{F} = \nabla \cdot \boldsymbol{\sigma}_{act}$ . To describe this effect and ensure  $\hat{\boldsymbol{n}}^2 = 1$ , we apply a relaxation equation in the Landau-Lifshitz-Gilbert form <sup>27</sup> for the director in the bulk,  $\partial_t \hat{\mathbf{n}} = -\hat{\mathbf{n}} \times \hat{\mathbf{n}} \times (a\hat{\mathbf{n}} + 2\gamma \mathbf{F})$ , where a is the director relaxation rate dependent on the director anchoring strength at the bounding plates and  $\gamma$  is a coefficient dependent on the surface anchoring strength at the bacterial body (see SI for details). the steady  $\hat{\mathbf{n}} = (\hat{\mathbf{n}}_0 + 2\gamma \mathbf{F} / a) / |(\hat{\mathbf{n}}_0 + 2\gamma \mathbf{F} / a)|$ ; substituting this expression into Eq. (3) and assuming  $|\mathbf{F}| \ll 1$ ,  $|n_y| \ll |n_x| \approx 1$  in the splay band, a general solution of the resulting equation is expressed in terms of the Lambert W function (product logarithm, see SI):

$$c^{\pm} = -\frac{W\left[-\frac{\gamma v_0 U_0}{a D_c} C^{\pm} \exp\left(\pm \frac{v_0 L}{\pi D_c} \cos \frac{\pi y}{L}\right) \cos \frac{2\pi y}{L}\right]}{\frac{\gamma v_0 U_0}{a D_c} \cos \frac{2\pi y}{L}}$$
(4)

here  $C^+ = C^- = C_0/2$  and  $C_0$  are determined from the condition  $\frac{1}{H} \int c(y) dy = \langle c \rangle$ , where  $\langle c \rangle \approx 0.3 \times 10^{14} \text{ m}^{-3}$ ;  $H \approx 10^3 \text{ }\mu\text{m}$  is the length of pattern along the *y*-axis. In the limit  $\gamma = 0$  (no realigning effect, or very dilute suspension),

$$c^{\pm} = C^{\pm} \exp\left(\pm \frac{v_0 L}{\pi D_c} \cos \frac{\pi y}{L}\right); \tag{5}$$

the y-dependence of the concentration  $c = c^+ + c^-$  is

$$c(y) = C_0 \cosh\left(\frac{v_0 L}{\pi D_c} \cos\frac{\pi y}{L}\right),\tag{6}$$

which explains the most salient feature of the experiment, namely, polar unidirectional flows in the splay regions and the absence of a net flow in the bend regions (Fig. 2h). However, numerical simulations show that a non-zero  $\gamma / a$  in Eq. (4) yields much sharper concentration peaks in the splay regions, and thus a better agreement with the experiment (Fig. 2d and Supplementary Fig. S1).

### Undulation of bacteria jets in concentrated dispersion

An intrinsic feature of active matter is the emergence of bending and splay instabilities and nucleation of topological defects at elevated activities <sup>1-3,11,28-32</sup>. Finding the means to suppress these instabilities and to convert activity into controllable steady flows might significantly expand the potential of active matter for applications <sup>2,7,31,32</sup>. Below we demonstrate that the patterned splay-bend stabilizes the bacterial flows.

In uniform cells,  $\hat{\mathbf{n}}_{\text{uniform}} = (1,0,0)$ , increasing the bacterial concentration above  $c_{\text{u}}^{\text{uniform}} \approx 0.9 \times 10^{14} \, \text{m}^{-3}$  leads to a bending instability of their trajectories (Supplementary Fig. S2 and Supplementary Video 2). In patterned cells of the same thickness  $h = 20 \, \mu \text{m}$ , however, the bacterial jets start to undulate only at  $c_{\text{u}}^{\text{s-b}} \approx 12 c_{\text{u}}^{\text{uniform}} \approx 11.8 \times 10^{14} \, \text{m}^{-3}$ ; the speed of bacteria in the jets remains nearly constant at  $10 \, \mu \text{m/s}$  below and above  $c_{\text{u}}^{\text{s-b}}$  (Supplementary Fig. S3a). At the onset of undulations, the contour length of the jet increases a bit faster than the number of bacteria in it, so that the concentration slightly decreases (Fig. 3c,d and Supplementary Fig. S3b). The stabilizing action of the splay-bend pattern is evident even at  $c > c_{\text{u}}^{\text{s-b}}$ , since the undulation preserves its wavelength,  $\lambda_{\text{u}} \sim 100 \, \mu \text{m}$ , and amplitude,  $A_{\text{u}} \sim 40 \, \mu \text{m}$  (Fig. 3a,b and Supplementary Video 3).

The stabilizing effect of the splay-bend pattern is caused by the increase of the elastic and interfacial energy when the undulating jets tilt with respect to the imprinted  $\hat{\bf n}_0$ . The angle  $\beta$  between the bacteria and  $\hat{\bf n}_0$  is mapped in Fig. 3e-g and Supplementary Fig. S3d-g. The standard deviation from 0 is significant,  $\Delta\beta = \sqrt{\sum_i \beta_i^2/n} \approx 36^\circ$ , where  $\beta_i$  is the angle measured for n bacteria in each frame (Supplementary Figs. S3-4). The nonzero  $\beta$  implies director twist along the z-axis, visualized by PolScope as diminished effective optical retardance, caused by the change of light polarization from linear to elliptical.

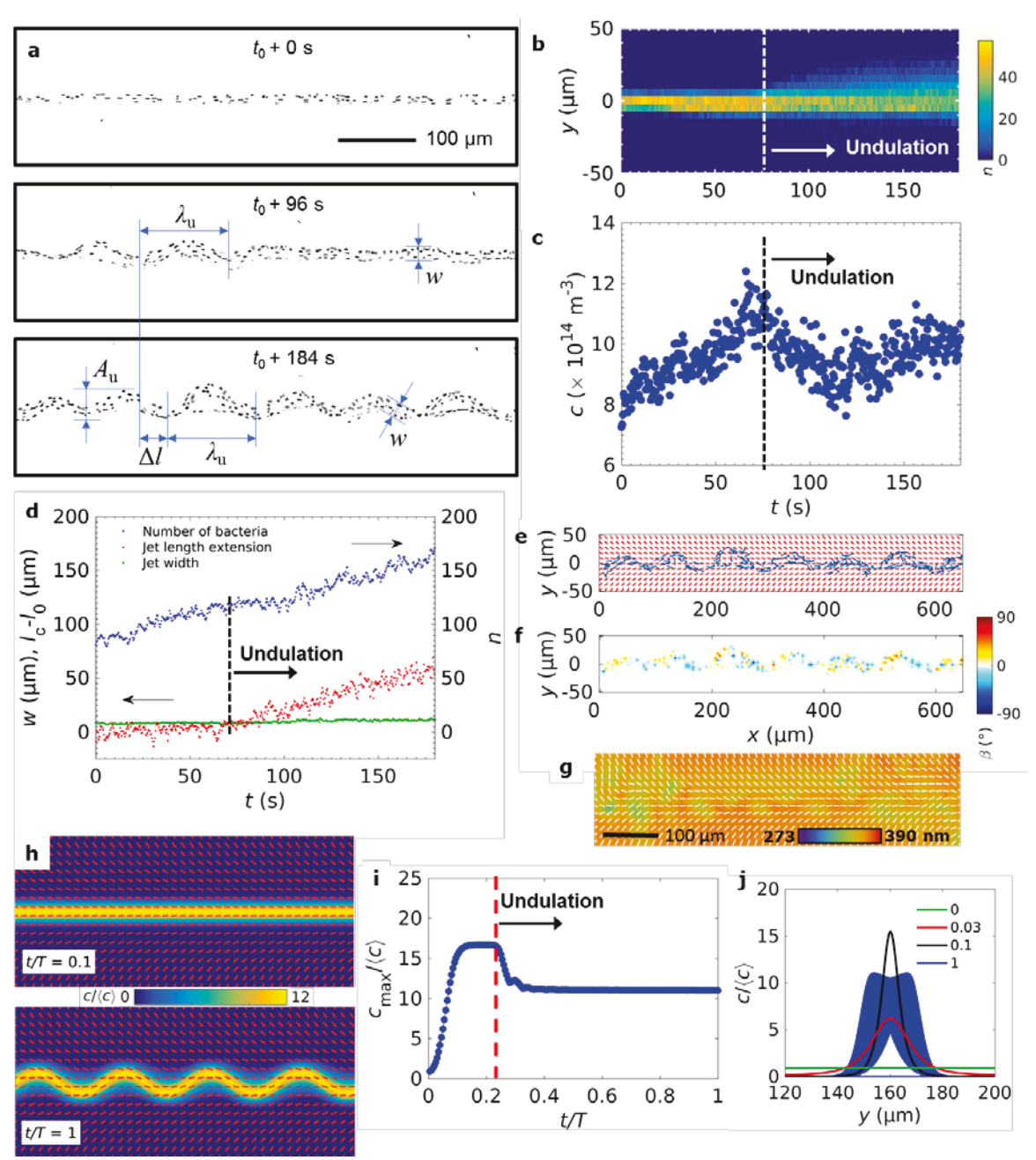


**Fig. 3.** Emergence of the bacteria jet undulations in concentrated dispersion,  $\langle c \rangle \approx 1.5 \times 10^{14} \text{ m}^{-3}$ . **a**, Microscopic images of bacteria at different stages of undulation development. The undulating wave translates from left to right with the speed  $\approx 0.3 \, \mu\text{m/s}$ . **b**, Kymograph of bacterial distribution along the *y*-axis with the time step 0.2 s; the color bar shows the number of bacteria per length step  $\Delta y = 5 \, \mu\text{m}$ . **c**, Time evolution of bacterial concentration in the developing jet. **d**, Total number of bacteria *n* in the jet, excess of the jet's contour length  $l_c - l_0$ , where  $l_0 = 650 \, \mu\text{m}$  is the length of the rectilinear jet, and average width *w* of the jet. **e**, Bacteria (blue arrows) and  $\hat{\bf n}_0$  (red ticks) in a fully developed undulation at time  $t_0 + 184 \, \text{s}$ . **f**, Map of the angle β between the bacteria and  $\hat{\bf n}_0$ . **g**, Optical retardation and the director map for an undulating instability imaged by PolScope.

**h**, Advection-diffusion simulation of  $\hat{\bf n}$  and normalized bacteria concentration  $c/\langle c \rangle$  for straight and undulating jets; parameters  $v_0=10~\mu\text{m/s}$ ,  $D_c=10~\mu\text{m}^2/\text{s}$ ,  $L=160~\mu\text{m}$ ,  $U_0=10^{-16}~\text{N}~\text{m}$ ,  $C_0=5.6\times10^{-14}~\text{m}^{-3}$ , and  $\gamma/a=7\times10^{-15}~\text{m}^3/\text{N}$ . **i**, Maximum bacteria concentration as a function of normalized computational time t/T, where T is the maximum simulation time. **j**, The simulated distribution of bacterial concentration in the splay region at different computation times (shaded blue for undulated jet, since concentration is x-dependent, from  $c_{\text{max}}=\max\left(c(x,y),x\right)$  to  $c_{\text{min}}=\min\left(c(x,y),x\right)$  obtained from simulation following Ref. <sup>10</sup>. See SI for the details of the simulation parameters.

The numerical simulations based on the model  $^8$ , demonstrate that the undulating jets indeed distort the director (Fig. 3h and Supplementary Video 4). The concentration of bacteria inside the jet increases rapidly and remains constant until the undulating jet is formed (Fig. 3i) after which it slightly decreases, similarly to the experimental observations in Fig.3c. The distribution of bacteria concentration becomes wider after the onset of undulations, Fig. 3j. The undulating wave propagates in the same direction as the bacterial jets with a typical velocity of  $0.5 \,\mu\text{m/s}$ , in agreement with the experiment (Supplementary Videos 3,4).

The dramatic difference in the concentration of bacteria in the splay and bend regions allows us to further extend the theoretical description by introducing a two-phase continuum model that captures the long-range hydrodynamic, collective flow interactions between the bacteria which result in the undulation. The two-phase model is intended to describe strongly concentrated regimes in which the bacteria-induced flows might be strong enough to override and significantly distort the orientation imposed by the background pre-patterned nematic. We do not assume that bacterial orientations closely match the nematic director, and hence are able to check whether the behavior is changed by such collective hydrodynamic interactions.

We define a phase-field order parameter  $\phi$  such that  $\phi=1$  demarcates the active regions occupied by bacteria and  $\phi=0$  the surrounding isotropic fluid. When  $\phi=1$  the nematic tensor  $\mathbf{Q}_b$  of the bacteria has a finite value, while  $\phi=0$  corresponds to the passive regions void of any activity with  $\mathbf{Q}_b=0$ . The dynamics of  $\phi$  is governed by a Cahn-Hilliard equation <sup>33</sup>, resulting in a diffuse interface between the active phase and the surrounding fluid <sup>34</sup> and it is coupled to the velocity field generated by active particles.

An important contribution to the orientation dynamics is the alignment of bacteria along the underlying director pattern. To model this, we contain all bacteria-nematic interactions in a Rapini-Papoular-like free energy term, which penalizes orientations of the active units that are not parallel to  $\hat{\bf n}_0$ . The preferred director orientation at the *B. subtilis* surface is tangential  $^{26}$ . Since the experiments are performed in a thin-film geometry,  $h \ll L$ , we use a depth-averaged approximation. The equations and simulation details are expanded upon in the SI.

The simulation is initialized with a stripe of active extensile phase placed along the y-direction in the splay-bend director pattern (Fig. 4a). As the simulation evolves, the initially uniform active stripe migrates to the splay region, and this migration continues until the bend region is completely devoid of the active phase. Consistent with the experiment and the analytical advection-diffusion model, once the active phase is focused within the splay region, a unidirectional flow persists towards the converging side of splay (Fig. 4a,b and Supplementary Video 5). The focusing can be interpreted in terms of active forces converging towards splay. In the bend regions, the forces are diverging, helping to deplete these regions.

The unidirectional jet starts to undulate once the activity is sufficient (Fig. 4c, Supplementary Fig. S5, and Supplementary Video 6). Consistent with the experiments, the underlying director pattern stabilizes the undulation with a well-defined final amplitude that depends on the activity (Fig. 4d). In the simulations, it is possible to increase the activity further. At high activities, the undulations continue to grow beyond the bend region in the background pattern, giving rise to an active turbulent state. Hence the model shows that the focusing and stable undulations persist even for large bacterial concentrations. In the SI we show that this conclusion persists even if the passive liquid crystal background can evolve in response to the active flow.

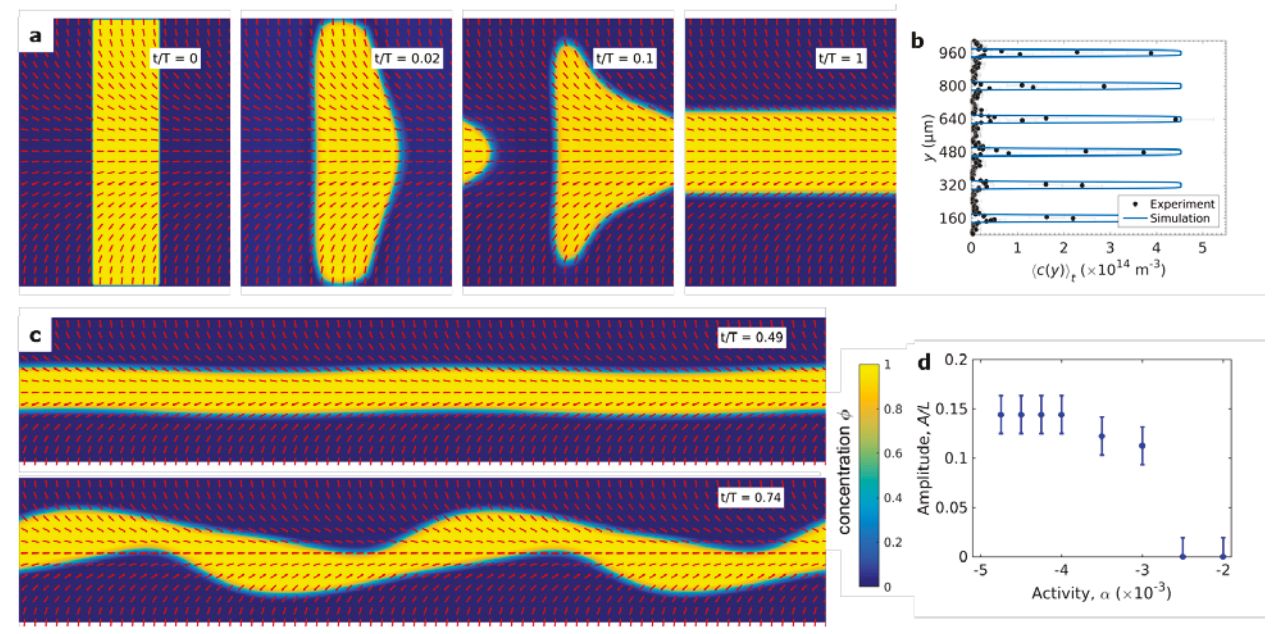


**Fig. 4.** Simulation results for the extensile living nematic ( $\alpha$  < 0) based on the two-phase model. **a**, The active nematic concentrates into splay region and moves from left to right. The simulation is initialized with a blob of active phase ( $\phi$ =1). The red solid lines show the directors of the background passive liquid crystal. **b**, Comparison of the experimental (dots; data for the dispersion with  $\langle c \rangle \approx 0.3 \times 10^{14} \text{ m}^{-3}$ ) and simulated (line) concentration profiles for pushers focusing into unidirectional jets within splay regions. The theoretical curves are normalized by the maximum concentration of swimmers in the splay regions. **c**, For higher activity, the jet starts to undulate. **d**, The steady-state amplitude of the undulation as a function of the dimensionless activity. The amplitude A is defined as the maximum height of the centre of the stripe. Error bars represent SD of the data.

The condensed bacterial jets can serve as effective micro-cargo transporters. As an example, Fig. 5 and Supplementary Videos 7-9 show transport of 5 µm diameter glass colloidal spheres by rectilinear jets (Fig. 5a-d), with a velocity in a range 1-7 µm/s (Fig. 5g,h) and by undulating jets (Fig. 5e,f). The splay-bend patterning in Fig. 5a-d allows one to transport micro-cargo along a well-defined y-coordinate in the xy-plane of the cell. This is an advantage over the unipolar transport reported earlier  $^{6,35,36}$  that does not select a particular y-coordinate. Considering the momentum  $p = mv_c$  of cargo, where m is its mass and  $v_c$  is its speed, the momentum transferred by the bacterial jets to a single colloid is  $p_{\text{single}} \approx 50 \times 10^{-20}$  kg m s<sup>-1</sup> and to a chain of six colloids  $p_{\text{aggreg}} \approx 200 \times 10^{-20}$  kg m s<sup>-1</sup> (Fig. 5a-d). These momenta are a few orders of magnitude higher than the momentum  $(0.001-2)\times 10^{-20}$  kg m s<sup>-1</sup> imparted by a single bacterium onto smaller particles  $^{35,36}$ . The calculated mean square displacement (MSD) of the single colloid

shows a strongly biased diffusion-advection transport along the jet of bacteria and confined diffusion in the perpendicular direction. Interpolation of the MSD along the x-axis with  $\left\langle \Delta x^2 \right\rangle = 2 D_{\rm eff} \Delta t^{\nu}$ , where  $D_{\rm eff}$  is the apparent diffusion coefficient, v is the apparent diffusion exponent, and  $\Delta t$  is the time-lag, yields  $v = 1.6 \pm 0.1$ , indicating the biased diffusion behavior of the sphere.

The biased diffusion persists at the time scales of the experiment (30 s) without any signs of reducing to normal diffusion. Thus, the patterned director field extends the apparent superdiffusion to the time scales much higher than the time scales limit of a few seconds observed for anomalous diffusion in an isotropic bacterial bath <sup>37,38</sup>.

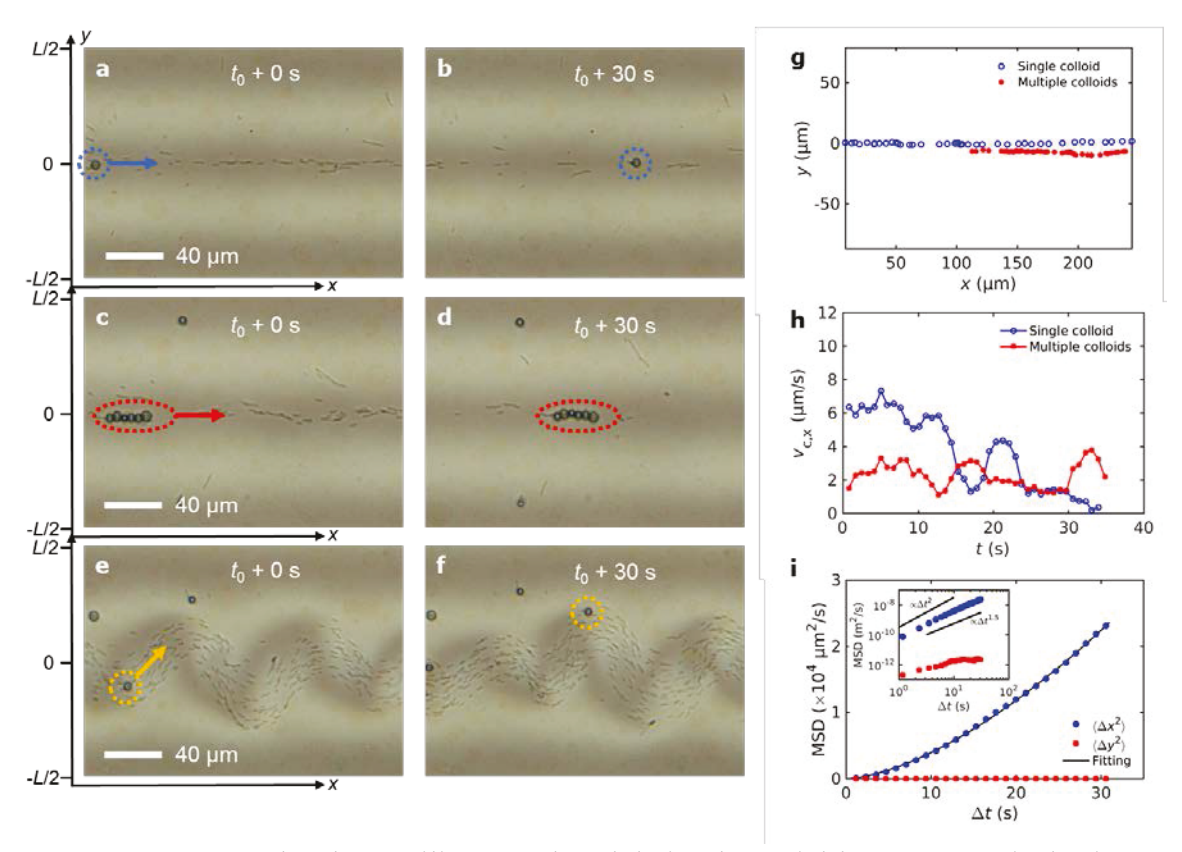


**Fig. 5**. Cargo transport by the rectilinear and undulating bacterial jets.  $\mathbf{a}$ , $\mathbf{b}$ , Optical microscope images taken 30 s apart of a single 5  $\mu$ m diameter glass sphere and  $\mathbf{c}$ , $\mathbf{d}$ , aggregate consisting of 6 glass spheres located in the splay region. The particles are relocated from left to right by the incoming unidirectional bacterial flow.  $\mathbf{e}$ , $\mathbf{f}$ , Colloidal particle carried by the undulating jet of bacteria.  $\mathbf{g}$ , Trajectories and  $\mathbf{h}$ , instantaneous horizontal velocity component of colloidal particles carried by the rectilinear jet.  $\mathbf{i}$ , Mean squared displacement (MSD) of the single colloid being transported by the jet in  $\mathbf{a}$ , $\mathbf{b}$ ; dashed line is the least square power fit to MSD along the x-axis.

In conclusion, we demonstrate the different roles of splay and bend in the patterned nematic director that controls collective motion of swimming bacteria. The bacteria engage in threshold-

less unidirectional collective motion along the splay bands, parallel to  $\mathbf{s} = -\hat{\mathbf{n}}_0 \nabla \cdot \hat{\mathbf{n}}_0$ . The focusing is explained by the aligning action of the underlying director onto the orientation of bacteria. The pre-imposed pattern makes the focusing persistent as the bacterial concentration increases. At very high concentrations, rectilinear jets start to undulate because of the hydrodynamic bend instability of interactive pushers. However, undulations are stabilized by the background director pattern and do not grow beyond the bend regions. The underlying nematic pattern thus prevents the instabilities of collective dynamics that are an intrinsic property of aligned polar self-propelled particles swimming in an isotropic environment <sup>11,29,30</sup>. Both unidirectional jet and undulating streams are capable of transporting colloidal particles, indicating possible future applications of this set-up in microfluidies and micro-cargo transport.

#### Methods

## Bacteria dispersion preparation

We use solution of disodium chromoglycate (DSCG) (purchased from Alfa Aesar), in aqueous solution of terrific broth (TB) medium (Sigma Aldrich) as a nematic host. TB solution serves as a growing and motility medium for Bacillus subtilis (strain 1085). The bacteria are inoculated from the lysogeny broth (LB) agar plate (Teknova) into the tube with 10 mL of TB and grown in a sealed tube to adapt the bacteria to oxygen starvation at 35°C inside the shaking incubator. The concentration of the bacteria is monitored with the custom-made optical density meter (based on Raspberry Pi 3 microcomputer). The tube with bacteria is extracted from the incubator before saturation of the bacterial concentration at 10<sup>13</sup> m<sup>-3</sup>. 0.1 mL of the liquid medium with bacteria is then centrifuged at 8000 rpm for 2.5 min and the medium is extracted upon which 0.1 mL of 14 wt% solution of DSCG in TB is added to the bacteria and carefully stirred with the pipet. The dispersion of B. subtilis in DSCG is used before the bacteria lost their swimming ability which is typically within 1-2 hours in a sealed cell without an oxygen supply. There are no changes in the concentration and velocity distribution of bacterial jets for at least one hour in multiple samples, Supplementary Video 10 and Supplementary Fig. S6. To obtain a concentration of bacteria above 10<sup>13</sup> m<sup>-3</sup>, we centrifuged 0.5 ml TB medium containing a high concentration of bacteria, extracted the TB and added 0.1 ml of DSCG to the tube and stirred it with the pipet. This bacterial suspension is injected into the cell and observed under the microscope.

## Sample preparation

For the photopatterned cells we clean soda-lime glass sheet about 1 mm in thickness in the ultrasonic bath with detergent at 60°C, rinse it with isopropanol and dry it in the oven at 90°C for 10 min. The glass is treated with UV-ozone in a sealed chamber for 10 min and is spincoated at 3000 rpm for 30 seconds with the azo-dye 0.5 wt% filtered solution of Brilliant Yellow (*Sigma Aldrich*) in dimethylformamide. The solvent is evaporated by annealing the glass substrates at 100°C for 30 min in the oven. The glass substrates with photoalignment layer are illuminated with a metal-halide X-Cite 120 lamp through the plasmonic photomask with a polarization map created by array of nanoslits. The substrates are cleaned with a compressed nitrogen gun, spincoated with toluene solution of 6.7 wt% reactive mesogen RM-257 (*Wilshire Tech.*) and 0.35 wt% photoinitiator Irgacure-651 (*Ciba*), illuminated with a 365 nm ultra violet lamp (UVL-56, 6 W)

for 30 min to completely polymerize reactive mesogen  $^{7,24}$ . Colloidal glass spheres used as cargo are purchased from *Bangs Laboratories*, *Inc.*; their mass density is  $\approx 2.2 \times 10^3$  kg m<sup>-3</sup>. The cells are sealed by the epoxy resin *Devcon*.

# Data acquisition and analysis

We use a Nikon TE-2000 inverted microscope with high resolution camera Emergent HR-20000C and  $20 \times$  magnification objective. The video sequences are recorded at 2 and 5 Hz rate. The sequences of images are analyzed by ImageJ2-Fiji <sup>39,40</sup>, particle image velocimetry MATLAB package <sup>38</sup> and custom written MATLAB code. To determine the local concentration dependence c(y), we count the bacteria from the microscopic images with enhanced contrast. The bacteria appear as higher intensity objects on a lower background intensity of the transparent liquid crystal field. We find the average image over all frames and subtract it from each frame of the video. With this the background liquid crystal intensity becomes even more suppressed and we segregate the individual bacteria using intensity thresholding technique. We then divide the number of bacteria in a narrow stripe of width  $\Delta y$  by the stripe volume  $\Delta V = \Delta yWh$ , where  $W = 736 \,\mu\text{m}$  is the width of the image along the x-axis. The concentration of bacteria in an undulating jet is calculated as the total number of bacteria n in the jet divided by the volume of the jet, which is proportional to its contour length  $I_c$  and width  $w: c = n/(wl_c h)$  (Fig. 3d and Supplementary Fig. S3b). PolScope microscope is a modification of a polarizing optical microscope with an electrically-controlled liquid crystal compensator; the instrument allows one to measure the local orientation of the inplane optic axis, which is also the director field, and optical retardance, see, for example, Ref. <sup>41</sup>.

#### Acknowledgement

This work was supported by NSF grants DMS-1729509 and CMMI-1663394. Research of I.S.A. was supported by the NSF grant PHY-1707900. K.T. was funded by the European Union's Horizon 2020 research and innovation programme under the Marie Sklodowska-Curie grant agreement No 722497. A. D. was supported by a Royal Commission for the Exhibition of 1851 Research Fellowship. We would like to acknowledge valuable discussions with J. Toner, V. Vitelli, and R. Green. We also thank S. Shiyanovskii and N. Aryasova who provided the Mathematica code for PolScope images analysis.

### **Author contributions**

T.T., R.K. and C.P. performed the experiments, T.T. performed experimental data analysis, A.D conceived the two-phase continuum model. K.T developed and performed the two-phase continuum simulations with inputs from A.D. and J.M.Y. M.M.G. performed advection-diffusion simulation, I.S.A. derived the analytical advection-diffusion model, H.Y. and Q.-H.W. provided the plasmonic photomask for patterned photoalignment, T.T. and O.D.L. wrote the manuscript with the input from all coauthors. O.D.L. conceived and supervised the project. All authors contributed to scientific discussions.

### **Competing interests**

The authors declare no competing interests.

## **Data availability**

The data represented in Figs. 2d, 2g-h, 3a, 3c, 3d, 3i-j, 4b, 4d and 5g-i are available as Source Data 2d, 2g-h, 3c, 3d, 3i-j, 4b, 4d and 5g-i. All other data that support the plots within this paper and other finding of this study are available from the corresponding author upon reasonable request.

### References

- 1 Marchetti, M. C. *et al.* Hydrodynamics of soft active matter. *Reviews of Modern Physics* **85**, 1143-1189 (2013).
- Doostmohammadi, A., Ignes-Mullol, J., Yeomans, J. M. & Sagues, F. Active nematics. *Nat Commun* **9**, 1-13 (2018).
- Zhou, S., Sokolov, A., Lavrentovich, O. D. & Aranson, I. S. Living liquid crystals. *P Natl Acad Sci USA* **111**, 1265-1270 (2014).
- 4 Smalyukh, I. I., Butler, J., Shrout, J. D., Parsek, M. R. & Wong, G. C. L. Elasticity-mediated nematiclike bacterial organization in model extracellular DNA matrix. *Phys Rev E* **78**, 030701 (2008).
- Kumar, A., Galstian, T., Pattanayek, S. K. & Rainville, S. The Motility of Bacteria in an Anisotropic Liquid Environment. *Mol Cryst Liq Cryst* **574**, 33-39 (2013).
- Mushenheim, P. C. *et al.* Effects of confinement, surface-induced orientation and strain on dynamic behavior of bacteria in thin liquid crystalline films. *Soft Matter* **11**, 6821-6831 (2015).
- Peng, C., Turiv, T., Guo, Y., Wei, Q.-H. & Lavrentovich, O. D. Command of active matter by topological defects and patterns. *Science* **354**, 882-885 (2016).
- 8 Genkin, M. M., Sokolov, A., Lavrentovich, O. D. & Aranson, I. S. Topological Defects in a Living Nematic Ensnare Swimming Bacteria. *Phys Rev X* 7, 011029 (2017).
- 9 Genkin, M. M., Sokolov, A. & Aranson, I. S. Spontaneous topological charging of tactoids in a living nematic. *New J Phys* **20**, 043027 (2018).
- Sokolov, A., Mozaffari, A., Zhang, R., de Pablo, J. J. & Snezhko, A. Emergence of radial tree of bend stripes in active nematics. *Phys Rev X* **9**, 031014 (2019).
- Aditi Simha, R. & Ramaswamy, S. Hydrodynamic fluctuations and instabilities in ordered suspensions of self-propelled particles. *Phys Rev Letters* **89**, 058101 (2002).
- Voituriez, R., Joanny, J. F. & Prost, J. Spontaneous flow transition in active polar gels. *Europhys Lett* **70**, 404-410 (2005).
- Giomi, L., Bowick, M. J., Mishra, P., Sknepnek, R. & Marchetti, M. C. Defect dynamics in active nematics. *Philos T R Soc A* **372**, 20130365 (2014).
- Thampi, S. P., Golestanian, R. & Yeomans, J. M. Vorticity, defects and correlations in active turbulence. *Philos T R Soc A* **372**, 20130366 (2014).
- Srivastava, P., Mishra, P. & Marchetti, M. C. Negative stiffness and modulated states in active nematics. *Soft Matter* **12**, 8214-8225 (2016).
- Putzig, E., Redner, G. S., Baskaran, A. & Baskaran, A. Instabilities, defects, and defect ordering in an overdamped active nematic. *Soft Matter* **12**, 3854-3859 (2016).
- Green, R., Toner, J. & Vitelli, V. Geometry of thresholdless active flow in nematic microfluidics. *Phys Rev Fluids* **2**, 104201 (2017).
- Maitra, A. *et al.* A nonequilibrium force can stabilize 2D active nematics. *P Natl Acad Sci USA* **115**, 6934-6939 (2018).
- Li, H. *et al.* Data-driven quantitative modeling of bacterial active nematics. *P Natl Acad Sci USA* **116**, 777-785 (2019).
- Wu, K. T. *et al.* Transition from turbulent to coherent flows in confined three-dimensional active fluids. *Science* **355**, eaal1979 (2017).

- 21 Ramaswamy, S. The Mechanics and Statistics of Active Matter. *Annual Review of Condensed Matter Physics* **1**, 323-345 (2010).
- Kumar, N., Zhang, R., de Pablo, J. J. & Gardel, M. L. Tunable structure and dynamics of active liquid crystals. *Science Advances* **4**, eaat7779 (2018).
- Joshi, A., Putzig, E., Baskaran, A. & Hagan, M. F. The interplay between activity and filament flexibility determines the emergent properties of active nematics. *Soft Matter* **15**, 94-101 (2019).
- Peng, C. *et al.* Patterning of Lyotropic Chromonic Liquid Crystals by Photoalignment with Photonic Metamasks. *Advanced Materials* **29**, 1606112 (2017).
- Volovik, G. E. & Lavrentovich, O. D. The Topological Dynamics of Defects Boojums in Nematic Drops. *Zh Eksp Teor Fiz*+ **85**, 1997-2010 (1983).
- Zhou, S. *et al.* Dynamic states of swimming bacteria in a nematic liquid crystal cell with homeotropic alignment. *New J Phys* **19**, 055006 (2017).
- 27 Aharoni, A. *Introduction to the theory of ferromagnetism*. Vol. 8 (Clarendon Press; Oxford University Press, 1996).
- Sanchez, T., Chen, D. T. N., Decamp, S. J., Heymann, M. & Dogic, Z. Spontaneous motion in hierarchically assembled active matter. *Nature* **491**, 431-434 (2012).
- Be'er, A. & Ariel, G. A statistical physics view of swarming bacteria. *Movement Ecology* 7, 1-17 (2019).
- 30 Saintillan, D. & Shelley, M. J. Instabilities and pattern formation in active particle suspensions: Kinetic theory and continuum simulations. *Phys Rev Lett* **100**, 178103 (2008).
- Guillamat, P., Ignés-Mullol, J. & Sagués, F. Control of active liquid crystals with a magnetic field. *P Natl Acad Sci USA* **113**, 5498-5502 (2016).
- Guillamat, P., Ignés-Mullol, J. & Sagués, F. Taming active turbulence with patterned soft interfaces. *Nature Communications* **8**, 1-8 (2017).
- Cahn, J. W. & Hilliard, J. E. Free Energy of a Nonuniform System .3. Nucleation in a 2-Component Incompressible Fluid. *Journal of Chemical Physics* **31**, 688-699 (1959).
- Blow, M. L., Thampi, S. P. & Yeomans, J. M. Biphasic, Lyotropic, Active Nematics. *Phys Rev Lett* **113**, 248303 (2014).
- Sokolov, A., Zhou, S., Lavrentovich, O. D. & Aranson, I. S. Individual behavior and pairwise interactions between microswimmers in anisotropic liquid. *Phys Rev E* **91**, 013009 (2015).
- Trivedi, R. R., Maeda, R., Abbott, N. L., Spagnolie, S. E. & Weibel, D. B. Bacterial transport of colloids in liquid crystalline environments. *Soft Matter* **11**, 8404-8408 (2015).
- Valeriani, C., Li, M., Novosel, J., Arlt, J. & Marenduzzo, D. Colloids in a bacterial bath: simulations and experiments. *Soft Matter* **7**, 5228-5238 (2011).
- Wu, X. L. & Libchaber, A. Particle diffusion in a quasi-two-dimensional bacterial bath. *Phys Rev Lett* **84**, 3017-3020 (2000).
- Tinevez, J. Y. *et al.* TrackMate: An open and extensible platform for single-particle tracking. *Methods* **115**, 80-90 (2017).
- Schindelin, J. *et al.* Fiji: an open-source platform for biological-image analysis. *Nature Methods* **9**, 676-682 (2012).
- Shribak, M. & Oldenbourg, R. Techniques for fast and sensitive measurements of twodimensional birefringence distributions. *Applied Optics* **42**, 3009-3017 (2003).